Desalination and Water Treatment
www.deswater.com

doi: 10.5004/dwt.2020.25016

179 (2020) 340–353
March

A comparison of ANN and RSM models for anionic dye adsorption onto bentonite-clay intercalated cobalt-aluminum LDH nanocomposites

Nuhu Dalhat Mu'azu[a,*], Nabeel Jarrah[b], Mukarram Zubair[c]

[a]*Department of Environmental Engineering, Imam Abdulrahman Bin Faisal University, 31451 Dammam, Saudi Arabia, Tel. +966507532689; emails: nmdalhat@iau.edu.sa/dalhat@gmail.com (N.D. Mu'azu)*
[b]*Department of Chemical Engineering, Mutah University, 61710 Karak 61710, Jordan, email: aljarrahn@mutah.edu.jo*
[c]*Department of Environmental Engineering, Imam Abdulrahman Bin Faisal University, 31451 Dammam, Saudi Arabia, email: mzzubair@iau.edu.sa*

Received 14 July 2019; Accepted 12 October 2019

ABSTRACT

The adsorptive performances for anionic dye, Eriochrome Black T (EBT), uptake from water using a hybridized aluminum-cobalt double layered hydroxide (LDH) and its clay intercalated nanocomposites were evaluated using response surface methodology (RSM). The predictive performances of the RSM models were compared with that artificial neural network (ANN) models developed using Bayesian Regulation algorithm considering root mean square error and coefficient of determination (R^2). The maximum removal efficiencies and adsorption capacities data obtained for the adsorbents well fitted cubic RSM models with insignificant lack of fit (R^2 = 0.991–0.997). The adsorption capacity increased with decrease in pH and increase in initial concentration of the EBT, while the temperature increase tends to decrease it. Respectively, the parent LDH maximum EBT adsorption capacity of 328.1 mg/g was significantly increased to 530 mg/g for the bentonite-clay intercalated LDH, both obtained at temperature 25°C, pH 2 and 100 mg/L initial EBT concentration. The bentonite-clay intercalated nanocomposite exhibited higher adsorption capacity for EBT compared with other adsorbents under similar operational condition. Even though, both the RSM and ANN models were reliable to interpret EBT adsorption by CO-Al-LDH and B-CoAl-LDH yet, higher values of R^2 of the ANN model (All R^2 = 0.999) and their corresponding lower values of the RSME indicate ANN better performances. The excellent reusability of the spent CO-Al-LDH and B-CoAl-LDH for three consecutive regeneration cycles indicates the high potentials bentonite hybridized LDH as an adsorbent for the uptake of dyes from industrial contaminated water and wastewater.

Keywords: Hybridized bentonite-clay layered double hydroxides; Cobalt-aluminum LDH nanocomposites; Anionic dye removal from water; Artificial neural network; Response surface methodology

1. Introduction

Layered double hydroxide (LDH) as novel material possessing brucite-like layers has recently been receiving increased research popularity for its broad range of uses in field of science and engineering [1–3]. Mostly, LDH are denoted with a structural formula $[M^{2+}_{(1-X)}\ M^{3+}_{(X)}\ (OH)_2]^{X+}\ [A^{n-}]_{X/n}.\ mH_2O$ [4]. M^{3+} represents trivalent cations (Fe^{3+} and Al^{3+}) and divalent cations (such as Mg^2, Ca^{2+}, Mn^{2+}, Co^{2+}, Fe^{2+}, Ni^{2+}, Zn^{2+}) are represented by M^{2+} within the brucite-like layers with intercalating anions A^{n-} which represents OH^-, F^-, NO^{3-}, Cl^-, CO_3^{2-} or SO_4^{2-} [4,5]. Characterized with large surface

* Corresponding author.

Presented at the Sixth International Conference on Water, Energy and Environment 2019 (ICWEE-2019), 26–28 March 2019, Sharjah, United Arab Emirates

area and high ionic exchange capacity and superlative structure, they are currently, considered as one of the most promising adsorbents for efficient removal of pollutants from water and wastewater [6,7]. Moreover, recent reviews show that applications of LDH have been advanced as a result of nanocomposites hybridization of LDH with other functional materials such as carbon materials, polymers or anions which further rendered having superior qualities employable for excellent water pollution control using adsorption process [7–9]. This has been demonstrated by several reported studies on using LDH nanocomposites such as CNT/MgAlO, MgAl, carbon dot/Mg-Al from which fast and enhanced adsorptive removal of several types of dyes and heavy metals were obtained [7,10–12]. Yet, research on discovering new LDH with high adsorptive performance would ensure identifying better novel materials characterized with higher uptake capacity for pollutants in water.

On the other hand, statistical based modeling technique, namely, response surface methodology (RSM) has been widely employed as a tool for designing experiments, developing models, evaluating influences and interaction between operating condition as well as determining process optimum conditions [13,14]. One outstanding benefit of RSM is that it requires fewer number of experimental trials compared with other statistical methods [13,14]. In recent years, artificial neural network (ANN) has been adopted as a modeling tool in various environmental applications which demonstrated clear predictive superiority over RSM [15–20]. This has been attributed to its power as a generic in structure and its possession historic data learning ability data. Moreover, as a contrast to RSM, ANN does not need specified function fitting. This implies that it is characterized by strong capabilities of universal approximation of a given response. As a technique in soft computing, ANN involves studying process via manipulation of network weights in order to capture a certain target response of interest [21]. Moreover, no any specific information of physico-chemical process affecting the system is required for its implementation.

Our recent works on LDH nanocomposites [7,22] as well as other relevant works suggest that study on evaluation of bentonite clay enhanced adsorptive performance of LDH composites via employing modeling approach such as RSM and ANN has so far not been reported. Moreover, most of the reported research mainly focused on using MgAl-LDH as the precursor material for removal of EBT [7,23,24]. Therefore, in this study, a new bentonite interlayed CoAl-LDH (B-CoAl-LDH) was synthesized using hybridization with bentonite via a ultrasonicated co-precipitation method. The produced nanocomposites were characterized for physicochemical and mineralogical composition using several techniques such as X-ray diffraction (XRD), X-ray fluorescence, thermal analysis (TG/TDA), scanning electron microscopy (SEM), Fourier transform infrared (FTIR), etc. RSM under different experimental conditions was employed for modeling, evaluating and optimizing the adsorptive performance of the adsorbents for aqueous sorption of Erichrome black T (EBT). The predictive performances of the RSM models were compared with that ANN models developed using Bayesian Regulation algorithm based on root mean square error (RMSE) and coefficient of determination (R^2).

2. Materials and methods

2.1. Materials

Commercial powdered bentonite (BDH, UK) of density 2.5 g/cm^3, cobalt(II) nitrate hexahydrate and all other chemical reagents used of high purity were purchased from Sigma-Aldrich CO, USA. Millipore Ultrapure system produced deionized water (DI) was used for stock solution of EBT dye (1,000 mg/L) preparation and all other purposes throughout the study.

2.2. Production and characterization of adsorbents

The CoAl-LDH synthesis, earlier reported method was adopted [25]. This involved mixing 0.01 mole $Al(NO_3)_3{\cdot}9H_2O$ and 0.03 mole $Co(NO_3)_2{\cdot}6H_2O$ in a 500 mL round bottom flask and adding 60 mL of water followed vigorous stirring at 600 rpm at 60°C for 15 min. The dropwise addition of 1 M NaOH was followed until pH was at 10 ± 0.5. Afterwards, the temperature was increased up to 90°C while stirring at higher speed of 1,000 rpm and refluxing for 24 h. Thereafter, the resulting suspension was centrifuged with ethanol. The resulting densed slurry was dried at 90°C for 24 h. For the synthesis of the B-CoAl-LDH, the Co-Al-LDH synthesis method was modified before the aforementioned coprecipitation reaction stage. About 500 mg bentonite added to 60 mL of DI water and ultrasonicated for 30 min at 60 rpm prior to the salt co-precipitation explained above. Characterization of the produced adsorbent was carried out using SEM, TEM, BET and detailed elsewhere [25].

2.3. Adsorption experimental design and tests

A 3^3 FC-CCD experimental design was adopted to investigate and model the influences of operational conditions *A* (25°C–45°C), *B* (20–100 mg/L) and *C* (2–6) with levels given in Table 1 selected based on our previous works [7,25]. As FC-CCD consists of a 3^k factorial runs, 2^k axial runs, and *k* central runs, a total of nineteen (19) batch adsorption tests were required as given in Table 2 were undertaken in duplicates. The tests were randomly run to ensure that influences of uncontrollable factors were avoided to ensure data quality [13,26]. Initially, two preliminary tests operated at temperature (25°C ± 5°C) were conducted using adsorbent mass of 5 mg by 40 mL of 100 mg/L EBT solution in 50 mL vails were agitated at 275 rpm for maximum of 4 h. Based on this test, an equilibrium time of 2 h for both adsorbents was established. Hence FC-CCD experimental runs were conducted with each sample vail containing 5 mg at the required temperature, initial EBT concentration

Table 1
RSM modeling experimental factors and their levels

Designation	Factor	Factors (coded) values		
A	Temperature, °C	25 (–1)	35 (0)	40 (+1)
B	EBT concentration, mg/L	20 (–1)	60 (0)	100 (+1)
C	Initial pH	2 (–1)	4 (0)	6(+1)

Table 2
RSM experimental for sorption of EBT onto Co-Al and B-CoAl

Test#	Operating conditions			Removal efficiency (%)		Adsorption capacity (mg/g)	
	Temperature (°C)	EBT concentration (mg/L)	Initial pH	CoAl	B-CoAl	CoAl	B-CoAl
	A	*B*	*C*	Y_1	Y_2	Y_3	Y_4
R1	25	20	2	83.50	88.95	133.60	142.32
R2	45	20	2	81.55	85.60	130.48	136.96
R3	25	100	2	41.01	66.25	328.08	530.00
R4	45	100	2	35.88	60.44	287.04	483.52
R5	25	20	6	5.90	13.00	20.72	52.40
R6	45	20	6	22.60	33.35	36.16	53.36
R7	25	100	6	2.17	4.15	17.36	33.20
R8	45	100	6	5.80	8.33	46.40	66.64
R9	25	60	4	12.05	15.87	57.84	76.16
R10	45	60	4	4.75	6.97	22.80	33.44
R11	35	20	4	20.45	33.70	32.72	53.92
R12	35	100	4	4.49	6.18	35.92	49.44
R13	35	60	2	52.97	69.65	254.24	334.32
R14	35	60	6	6.27	13.88	30.08	66.64
R15	35	60	4	7.83	9.73	37.60	46.72
R16	35	60	4	5.03	10.42	24.16	50.00
R17	35	60	4	7.40	9.25	35.52	44.40
R18	35	60	4	6.32	11.03	30.32	52.96
R19	35	60	4	7.25	10.58	34.80	50.80

and initial pH and agitated at 275 rpm for 2 h. After each run, the residual EBT dye solution was separated from the spent adsorbent operated at 4,000 rpm for 10 min via centrifuge. The EBT residual concentration was measured using spectrophotometer (Hach Lange λ = 530 nm). The target responses, EBT removal efficiency and adsorption capacity for each of the samples were estimated using Eqs. (1) and (2).

$$q_e = \frac{C_0 - C_e}{W} \times V \tag{1}$$

$$R = \frac{C_0 - C_e}{C_0} \times 100 \tag{2}$$

2.4. RSM modeling

RSM was adopted because it has been known for its effectiveness as initial steps in evaluation and assessment of processes using fewer experimental samples. RSM facilitates development of response models that incorporates curvature easing process optimization while integrating ANOVA [26,27]. Additionally, it enables easy correlating the operational parameters and their interactive effects on the targeted responses. To evaluate the impact of the bentonite incorporation into CoAl-LDH on EBT adsorption was modeled via RSM modeling under the 3^3 FC-CCD. Development of RSM models was based on fitting data into Eq. (3) with the aid of Design-Expert 8.0 statistical program [28].

$$y = \beta_0 + \sum_{i=1}^{k} \beta_i x_i + \sum_{i=1}^{k} \beta_i x_i^2 + \sum_{i=1}^{k-1} \sum_{j=2}^{k} \beta_{ij} x_i x_j + \varepsilon \tag{3}$$

2.5. ANN models development

The ANN models for adsorption data (Y_1, Y_2, Y_3 and Y_4) were developed using a two-layer under the MATLAB™ (R2017a) environment according to the generalized architectural ANN scheme as depicted in Fig. 1. The best ANN models were obtained based on the optimal number of neurons that yielded the best performances via balancing between training, validation and test data which were split 70%, 15% and 15%, respectively. Three suitability of the ANN-based algorithms namely scaled conjugate gradient, Bayesian Regularization (BRA) and Levenberg–Marquardt algorithm (LMA) were initially tested for the whole data set. Based on preliminary assessments, the BRA was observed to be the most suitable algorithm for the FC-CCD adsorption data set due to its clear better performances. Consequently, the BRA was adopted for optimizing and training the ANN models.

2.6. Evaluation of developed models performance

In order to ensure common parameters were used in facilitating understanding attained RSM and ANN models accuracy and reliability, the performances of the developed

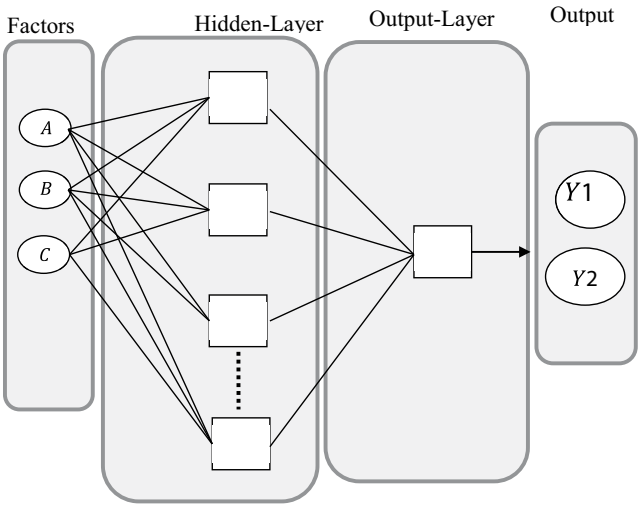

Fig. 1. ANN model structure.

RSM and ANN models were evaluated using coefficient of determination ($0 < R^2 < 1$) and RSME according to Eqs. (4) and (5), respectively.

$$R^2 = 1 - \frac{\left(y_i - y_i'\right)^2}{\left(y_i - \bar{y}\right)^2} = 1 - \frac{\text{SSR}}{\text{SST}} \tag{4}$$

$$\text{RMSE} = \frac{1}{n}\sum_{i=1}^{n}\left(y_i - y_i'\right)^2 = \frac{1}{n}\sum_{i=1}^{n}\text{SST} \tag{5}$$

y_i, $\bar{y}$ and y_i' represent the experimental, mean and predicted responses, respectively. SSR is the sum of squares for estimated errors also known as residuals; SST is the total sum of squares, which represents the total variation of the dependent variable around its mean value. The closer the R^2 value to 1, the higher its predictive capabilities while zero-value indicate random relationship. On the other hand, low values for RMSE are desirable with zero-value indicating model with no predictive error.

3. Results and discussion

3.1. Adsorbents characterization analysis

The SEM image of parent CoAl-LDH and the hybrid B-CoAl-LDH adsorbents are given in Fig. 2a which for both indicate roughly, compacted surfaces of homogeneous nanoparticles [29]. However, it could be seen that the composite B-CoAl-LDH (Fig. 2b) possessed marginally different morphology of softer nanostructure with possible higher porosity with better uniformity. These suggest that there was a success in dispersing and also intercalation of the bentonite particles within the precursor CoAl to produced the composite B-CoAl-LDH using the co-precipitation method. To further confirm, the excellent intercalation of bentonite within the layers of CoAl LDH nanoparticles EDS and BET surface area analyses were undertaken and presented as supplementary materials in Fig. S1 as well as Tables S1 and S2. Incorporation of the bentonite was found to have led to

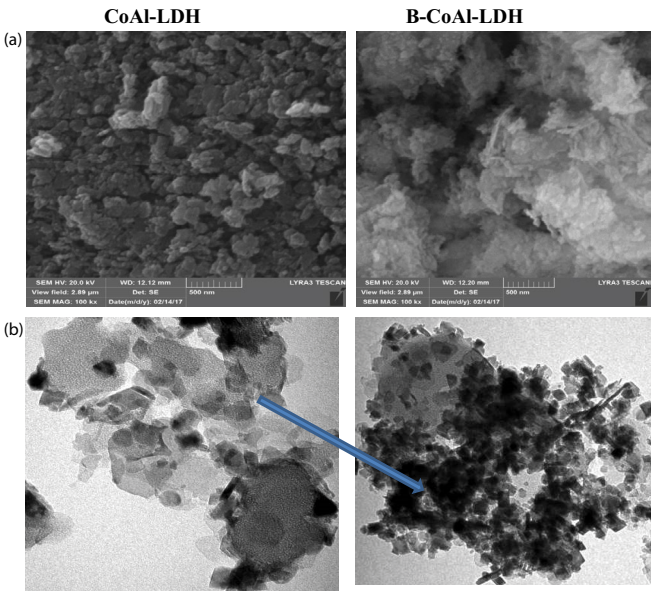

Fig. 2. (a) SEM micrographs and (b) TEM for CoAl-LDH and B-CoAl-LDH.

significant higher B-CoAl-LDH composite BET surface area of 119.14 m^2/g compared with 44.20 m^2/g for the CoAl-LDH (Table S1). Likewise, addition of bentonite resulted in substantial reduction in pore size of B-CoAl LDH (19.51 A°) relative to CoAl (34.61 A°) as given in Fig. S1 and Table S1. Nevertheless, pore size and pore volume for both show the mesoporous surface characteristics of the two adsorbents [12,22,30]. Additionally, the EDS analysis results given in Table S2 show that the elemental composition in the bentonite, omitted in the precursor LDH, are clearly manifested in the bentonite-Co-Al [22]. Also, Fig. 2b for the B-CoAl-LDH TEM analyses reveals a successful ultrasonicated hydridization of homogenous high porous bentonite nanoparticles intercalated into the interlayers of the CoAl-LDH which could yield higher adsorptive performance.

Fig. 3 shows the % weight loss of bentonite-CoAl at varied temperature 20°C–750°C. It was observed that the percentage weight loss at 20°C–200°C correspond to water molecules was around (20%–23%). Moreover, the % weight loss of bentonite-CoAl further reduced to 24%–54%, at temperature 200°C–400°C, respectively. This is related to the degradation of oxygen based functional groups (hydroxyl, carbonyl and carboxylic) on surface of composite. Higher % weight loss clearly suggests the abundant presence of functional groups which is in agreement with FTIR analysis. Further increase in temperature from 400°C to 700°C showed a minimal decrease of about 5% weight loss of composite. Similarly, thermal behavior of the precursor CoAl-LDH showed comparable behavior as reported in our previous study [12,25]. Thus, these are indicative of good characteristics with great potentials for the B-CoAl to exhibit higher adsorptive performance for EBT removal from aqueous system [12].

3.2. Development of RSM models for EBT sorption

The experimental data provided in Table 2 are the calculated average values of R and q_e for the duplicated 38

adsorption tests. The values of these adsorption parameters ranged between 2.17% to 83.5% and 17.36 to 328.08 mg/g for CoAl-LDH. However, for the hybrized B-CoAl-LDH, the corresponding values obtained were 4.15% to 88.95% and 33.2 to 530 mg/g, respectively. These values indicate significant performance improvement the ultra-sonicating of the CoAl-LDH with bentonite. Thus, a multiple nonlinear regressions was employed to fit data in Table 2 into Eq. (1). The best RSM arrived at according to high significant model's terms with no alias and p-value < 0.0001 (Table 2) were reduced cubic models in Eqs. (6)–(9), respectively [31]. These models include only terms possessing significant influence on respective response as indicated by the ANOVA performed at p-values < 0.05 (Table 2) [26]. For instant, considering the ANOVA of Y_1, all the single terms (i.e., main effects A to C) and their two-way interaction effects AB, AC and BC, B^2 and C^2 squared effects as well as cubic term A^2B and AB^2 are significant model terms. Even though the A^2 terms were insignificant (p-value = 0.5113), they exerted significant influence when interacted in the cubic term A^2B (p-value = 0.0093), as such contributed in the accuracy in the models prediction. Similarly, interpretation of the other developed RSM models can be deduced according to the respective model Eqs. (4)–(6) and ANOVA in Table 2.

3.3. EBT adsorption Pareto charts

The comparative assessment of the contributions of the main as well as the two-way interactions of the operational conditions on the investigated responses is pictorially provided by the Pareto charts presented in Figs. 4a and 5a. Hence, the parameters relative importance on the responses Y_1 to Y_4 are proportionally represented by the Pareto's plot height; the higher the bar the higher the influence [13]. Consequently, factor C, B and their interacting effects BC mainly controlled adsorption of EBT onto adsorbents for responses Y_1 (Fig. 4a), Y_3 and Y_4 (Fig. 5a). Meanwhile for Y_2 in Fig. 4a, the Pareto's analysis suggests that AC and AB had higher contributions compared with BC. Consistently, these plots revealed that in absence of its interactions, factor A had the least influence on EBT adsorption for both adsorbents. This Pareto's analysis consistently corroborates the ANOVA presented in Table 3.

$$Y_1 = 7.12 - 3.65A - 7.98B - 25.22C - 2.03AB + 3.43AC + 8.45BC + 0.83A^2 + 4.90B^2 + 22.05C^2 - 5.61A^2B + 5.31AB^2 \quad (6)$$

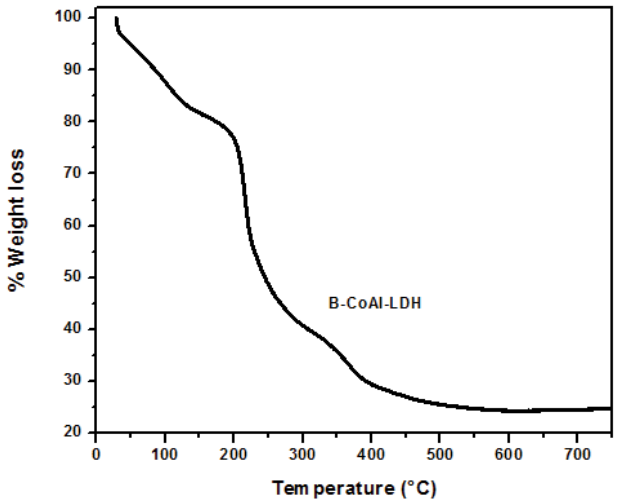

Fig. 3. TGA for B-CoAl-LDH.

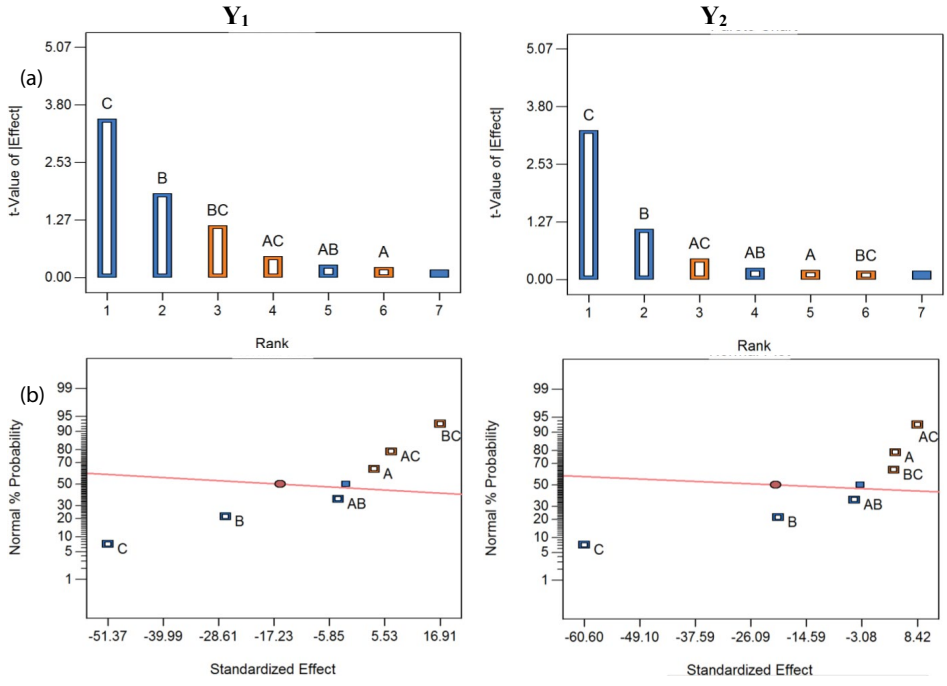

Fig. 4. Pareto diagram and probability normal plot of (a) CoAl and (b) B-CoAl for EBT removal efficiency.

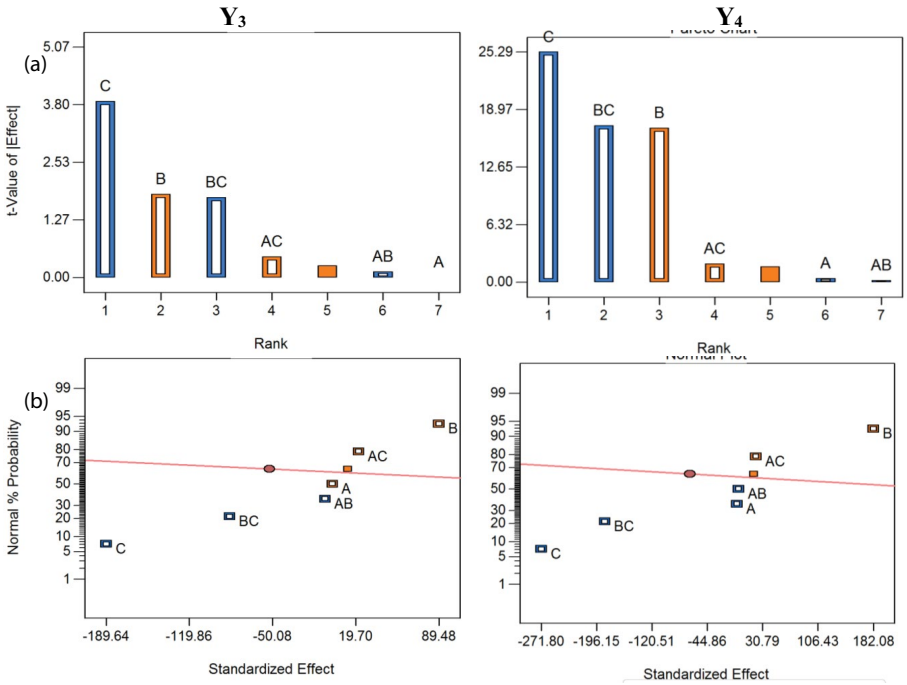

Fig. 5. (a) Pareto diagram and (b) probability normal plot of CoAl-LDH and B-CoAl-LDH for EBT adsorption capacity.

Table 3
ANOVA of CoAl-LDH and B-CoAl-LDH for EBT sorption models

	Y_1		Y_2		Y_3		Y_4	
	F-value	*p*-value	*F*-value	*p*-value	*F*-value	*p*-value	*F*-value	*p*-value
Model	270.87	<0.0001	171.00	<0.0001	136.97	<0.0001	482.22	<0.0001
A	6.70	0.0360	3.56	0.0886	3.94	0.0752	8.55	0.0152
B	32.03	0.0008	107.21	<0.0001	0.03	0.8597	0.09	0.7654
C	1,599.45	<0.0001	798.60	<0.0001	620.10	<0.0001	1719.47	<0.0001
AB	8.30	0.0236	3.90	0.0766	–	–	–	–
AC	23.62	0.0018	12.74	0.0051	6.31	0.0308	8.71	0.0145
BC	143.80	<0.0001	–	–	95.07	<0.0001	641.44	<0.0001
A^2	0.48	0.5113	–	–	–	–	–	–
B^2	16.53	0.0048	11.15	0.0075	–	–	–	–
C^2	334.19	<0.0001	223.80	<0.0001	267.52	<0.0001	858.06	<0.0001
A^2B	12.65	0.0093	–	–	–	–	–	–
A^2C	–		–	–	3.17	0.1055	5.51	0.0408
AB^2	11.33	0.0120	5.83	0.0364	–	–	–	–
BC^2	–	–	–	–	19.12	0.0014	130.40	<0.0001

[a]Significance established at 5% (*p*-value < 0.05).
[b]Significance established at 10% (*p*-value < 0.1).
LOF = lack of fit.

$$Y_2 = 11.24 - 4.45A - 10.93B - 29.82C - 2.33AB + 4.21AC + 6.27B^2 + 28.10C^2 + 6.37AC^2 \quad (7)$$

$$Y_3 = 34.63 - 17.52A + 1.60B - 98.27C + 11.08AC - 43.02BC + 93.78C^2 + 17.56AC^2 + 43.14BC^2 \quad (8)$$

$$Y_4 = 50.87 - 21.36A - 2.24B - 135.49C + 10.78AC - 92.52BC + 139.06C^2 + 19.18AC^2 + 93.28BC^2 \quad (9)$$

3.4. Validation of EBT sorption RSM models

The developed CoAl-LDH and B-CoAl-LDH EBT sorption models' coefficients of determination (R^2) of 0.998, 0.991, 0.993 and 0.997 for Y_1, Y_2, Y_3 and Y_4, respectively, are very high and not far from their respective R^2-adjusted and R^2-predicted. This indicates strong agreements amongst all the models biased and non-biased regression coefficients as

required in RSM modeling [26]. Thus, the developed RSM models' are characterized by high prediction capabilities of the experimental data [32,33]. The plots of the normal probability presented in Figs. 4b and 5b are linear, indicating normally distributed experimental data. Besides, considering the various sources models variations based on their calculated *F*-values from ANOVA, all the model terms are statistically significant (i.e., $p < 0.05$ or $p < 0.1$ in Table 3). These diagnostics imply the appropriateness of using the developed RSM models for understanding the influence of the operating conditions on EBT sorption onto the two adsorbent for drawing reliable inferences [26,27].

3.5. Effect of adsorption parameters on EBT removal and adsorption capacity

Based on constructed 3D plots developed from the developed RSM models (Figs. 6 and 7), the influence of operating conditions on EBT removal from water are discussed below.

3.5.1. Effect adsorption operating parameters on EBT removal efficiency

Fig. 6 depicts the combined effects of the operating conditions on EBT removal efficiency for the two adsorbents. Apparently, for both CoAl and B-CoAl, increase in the initial pH of the EBT contaminated water from 2 to 6 profoundly led to decrease in the percentage removal of EBT with the highest obtainable removals occurring at pH 2 (Figs. 6a and b). At fixed 20 mg/L EBT and temperature 25°C, the highest removal efficiency of and 83.5% and 88.95% deteriorated to as low as 5.9% and 13% when the initial pH was increased from 2 to 6, respectively. This corroborates other studies of LDH which reported that higher pH values do not favor EBT (as well as other dyes) adsorption [34–36]. In fact, most of these studies found that the optimal LDH adsorption capacity was achieved at pH 2 despite the tendency for LDH instability due to possible solubilisation. As such, this was ascribed to adding more OH^- ions as the pH increase, thereby dwindling the chances

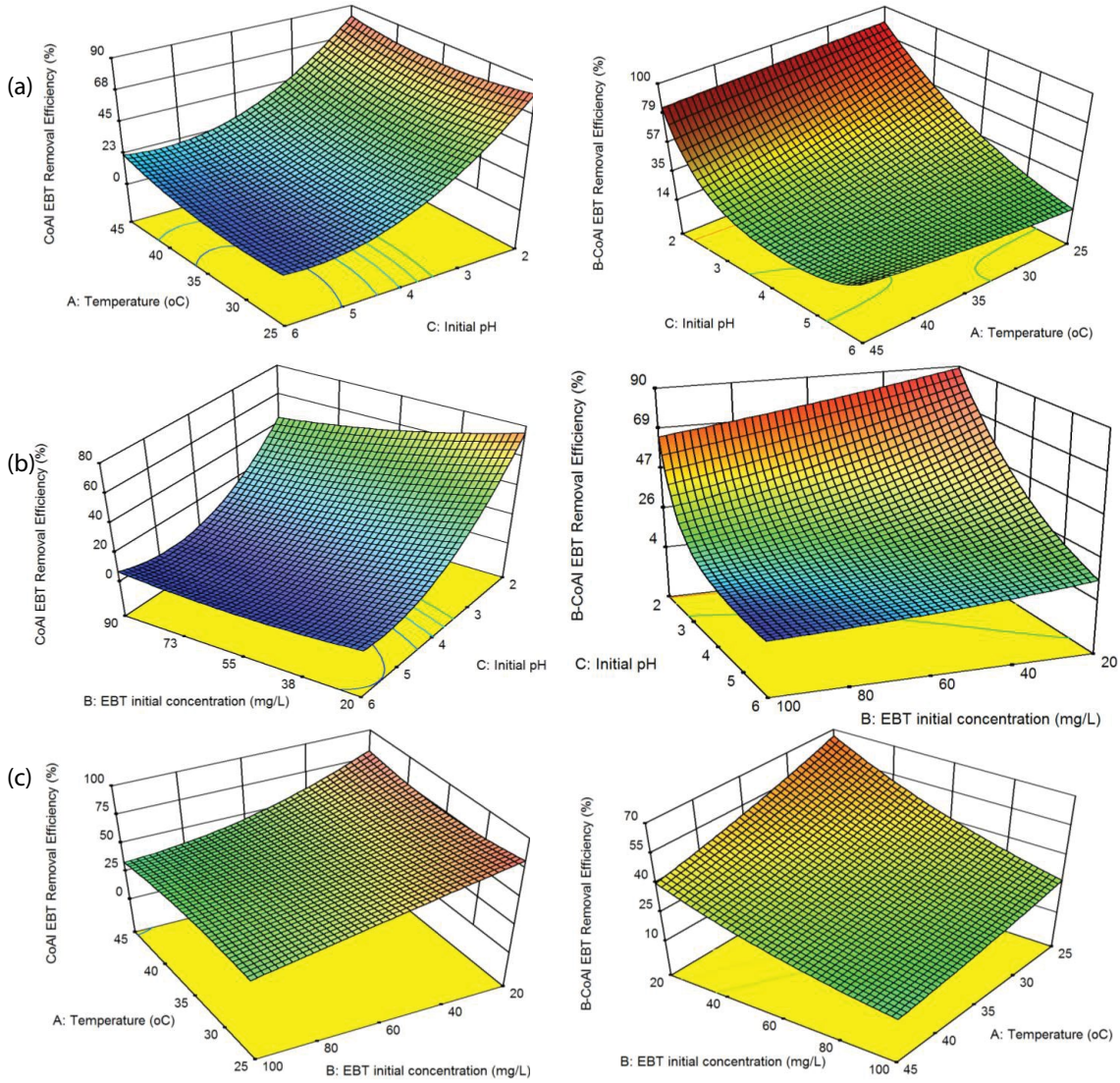

Fig. 6. Effect of operational conditions on EBT removal efficiency for (a) CoAl-LDH and (b) B-CoAl-LDH.

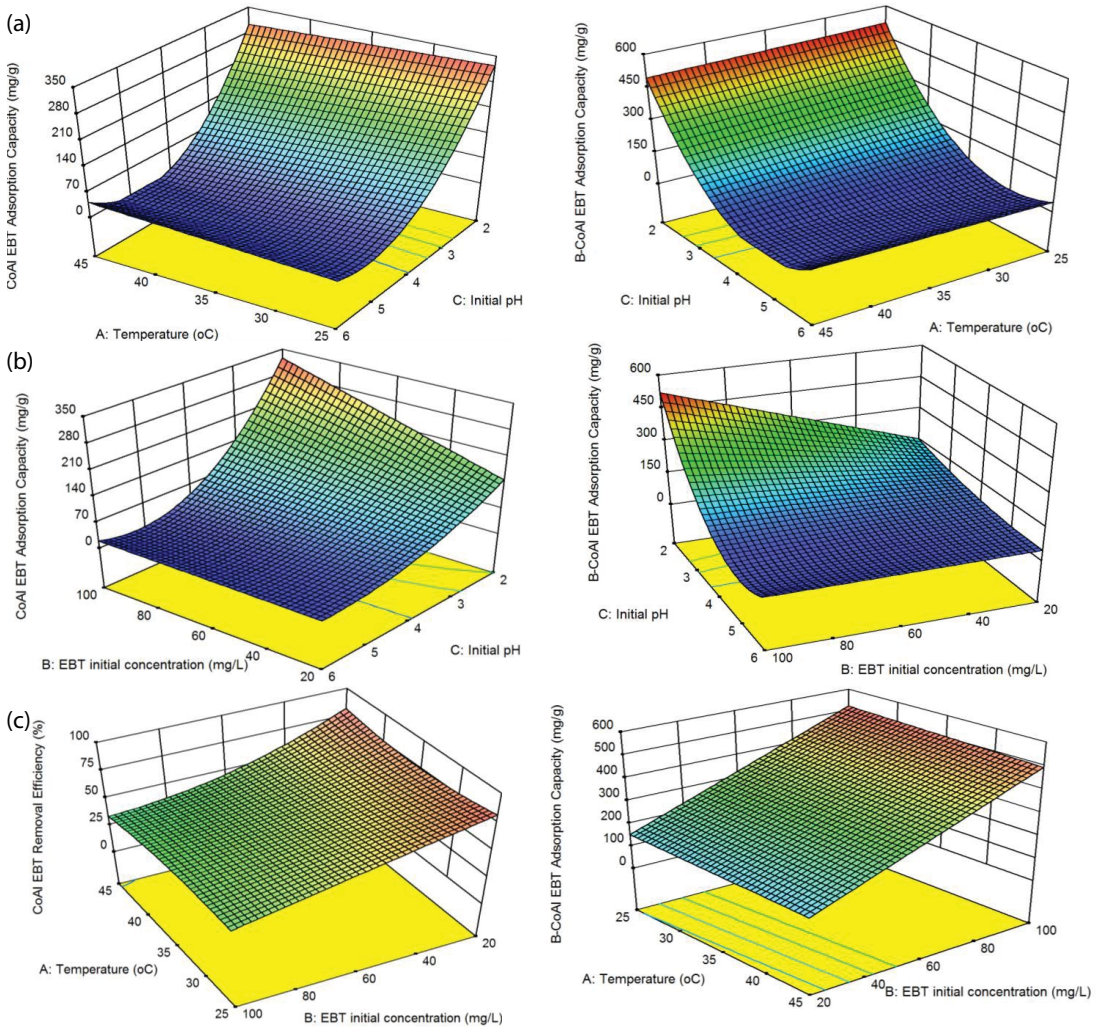

Fig. 7. Effect of operational conditions on EBT adsorption capacity for (a) CoAl-LDH and (b) B-CoAl-LDH.

for the anionic EBT interactions to the functional groups on surfaces of the two adsorbents [37]. Lower solution pH promotes protonation of the adsorbents surface functional groups, thus, resulting in stronger electrostatic attraction of the anionic EBT to the CoAl and B-CoAl, thereby increasing the removal efficiency [38]. Supportively, the two adsorbents point of zero charge (PZC) measured using drifting method were found to be above pH 2 (around 4.8 and 5.2, respectively), which suggests that, at pH 2 (<PZC), protonation occurring at the adsorbents surfaces was highly promoted [38]. Consequently, at pH 6, which was above the PZC values for both the adsorbents, their surface became negatively charged which was more prone to resist the anionic EBT ions, thus, the dramatic observed dropped in the EBT removal efficiencies [39].

The dependency of the initial EBT concentration on the removal efficiency for the two adsorbents (Y_1 and Y_2) is displayed in Figs. 6b and c (and also Table 3). Similarly, as the initial concentration was increased from 20 to 100 mg/L at fixed initial pH 2 and temperature 25°C, the maximum removal efficiency decreased from 83.5% to 35.88% and 88.9% to 66.4% for the CoAl and B-CoAl, respectively. These marked influences by the pH and initial EBT concentration corroborate a stronger interaction that existed between these two parameters when compared with the interactive effects as observed earlier. Contrastingly, the EBT removal efficiency for both adsorbents slightly decreased when temperature was increased which is more manifested for the B-CoAl for its higher adsorptive performance (Fig. 6c). Even though, changing the temperature was found to also influence the EBT removals for both the tested adsorbents, yet, its effect was the least amongst the investigated parameters (Fig. 6c and least *p*-values in Table 3). Moreover, the temperature exhibited lower interactive effects with other parameters on the measured responses.

3.5.2. Effect of adsorption operating parameters on sorption capacity

The influence of investigated operating conditions on EBT sorption capacities for both adsorbents is depicted in Fig. 7. The clear trends in Figs. 7a and b reveal that uptake

capacity increased with decrease in pH. Conversely, when the initial EBT concentration was increased, the adsorption capacity also increases in spite of the earlier observed decrease in removal efficiencies (Fig. 6b). Increase in temperature was susceptible to reduce both the removal efficiency and adsorption capacity, thus, indicating an exothermic process. The maximum achievable EBT adsorption capacity was profoundly raised by a factor of 2.5 and 3.75 to 328.8 mg/g and 530 mg/g for an increase in the EBT initial dye concentration from 20 to 100 mg/L, respectively. Apparently, the influence of temperature is not conspicuous from the 3D plots as it is apparently dwarfed due to its least influence as observed earlier for the removal efficiencies (Fig. 7c). However, based on the developed models, ANOVA as well as Pareto charts presented earlier. The overall optimal adsorption capacity was obtained at 25°C, pH 2 and 100 mg/L EBT for both adsorbents. This notable continuous enhancement in the adsorption capacity of the adsorbents at the fixed adsorbents dosage when the initial concentration was increased was attributed to increase in potentials of higher interactions between the available adsorption active sites as more EBT molecules are introduced into the solution [40]. Moreover, the improvement in the measured adsorptive characteristics for the B-CoAl was hence manifested in the observed higher q_e for B-CoAl. However, observed maximum adsorption capacities for both the two adsorbents which occurred at pH, initially decreases at higher rates until, apparently, observed a decline beyond the PZC (Figs. 6a and b).

FTIR analyses were performed and given in Fig. 8a for both two adsorbents before and after the dye adsorption process showed shifts in symmetric stretching interlayer of NO_3^- at 1,292 and 1,358 cm^{-1}, at peak 1,750–1,642 cm^{-1} for C=O as well as the disappearance and intensity reduction for bands at 1,217 cm^{-1} and 1,001 intensity for Si–O–Si and Si–O. Similarly, XRD peaks for the bentonite intercalated nanocomposites analyzed after EBT uptake show (Fig. 8b) the existence of the EBT ions considering the interlamellar space of the B-CoAl-LDH, there was an increase slightly to 0.728 nm (2θ = 12.140) from 0.778 nm (2θ = 11.360) for the 003 basal spacing [12,25]. These changes were credited to EBT anion molecules exchange with other LDH anions [12].

3.6. Adsorption models' performances: ANN vs. RSM

RSM and ANN have recently been popular techniques for modeling sorption process in literature because of their potentials of providing good relationships between the parameters and target responses. Both approaches are powerful in capturing complex nonlinear relations [17]. For that, RSM and ANN techniques were employed for modeling CoAl and B-CoAl EBT adsorption and removals from aqueous solution using the same experimental data obtained based on the FC-CCD (Table 3). Table 4 shows that the overall ANN models optimal performances during the development of the ANN models were obtained at number of neurons = 10 which was attained via balancing between individual performances of the training and test data sets as given in the table. The comparative performances of the RSM and ANN are compared for the Y_1, Y_2, Y_3 and Y_4 models in terms of residuals (predicted-experimental), R^2 and RMSE are shown in Table 5. Obviously, the larger absolute residuals are attributed to the RSM models compared with the ANN models. This resulted in both higher values of R^2 = 0.999 for all the ANN four models. Even though, the R^2s for the RSM models were also comparatively high, yet, considering the lower values of the RSME of the ANN

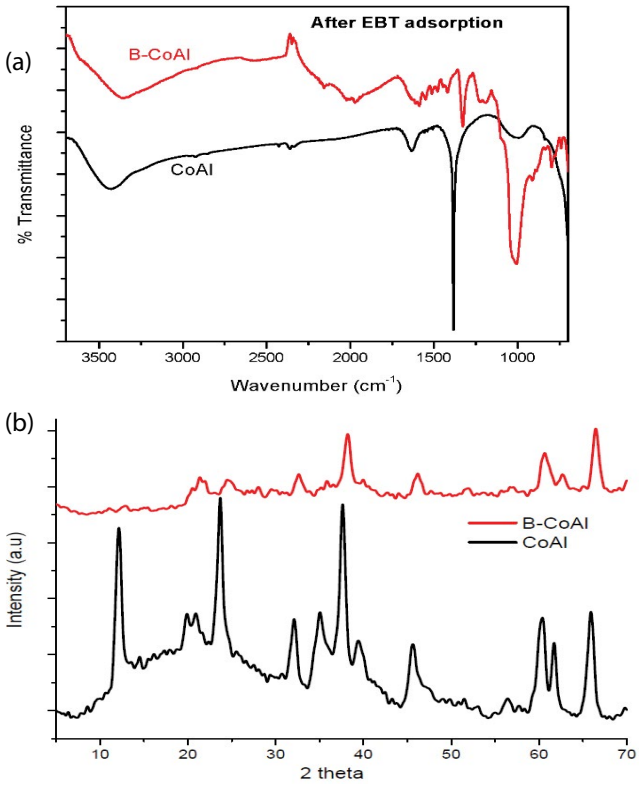

Fig. 8. (a) FTIR spectra and (b) XRD after EBT adsorption for CoAl-LDH and B-CoAl-LDH.

Table 4
Developed ANN models optimal performances

Model	No. of neurons	Training		Testing		Overall	
		R^2	RMSE	R^2	RMSE	R^2	RMSE
Y_1	10	0.999	0.1897	0.996	2.8	0.999	0.776
Y_2	10	0.999	0.072	0.999	34.17	0.997	2.336
Y_3	10	0.999	1.00023	0.918	86.033	0.999	3.798
Y_4	10	0.999	0.299	0.998	50.927	0.999	2.879

Table 5
RSM and ANN predictive models residuals (predicted minus experimental)

Test#	Removal efficiency, %				Adsorption capacity, mg/g			
	Y_1		Y_2		Y_3		Y_4	
	RSM	ANN	RSM	ANN	RSM	ANN	RSM	ANN
R1	–1.6	0.16	–2.63	0.01	16.36	–0.07	12.5	0.00
R2	0.87	0.15	0.8	0.01	–2.6	–0.06	–8.06	0.01
R3	0.87	0.07	2.87	0.00	–2.6	0.01	–8.06	0.03
R4	–1.6	0.01	–0.56	0.00	16.36	0.05	12.5	0.01
R5	1.8	0.06	5.26	–0.01	–3.42	–0.04	–5.08	0.00
R6	–0.66	0.13	1.83	0.02	3.38	0.06	11.16	0.01
R7	–0.69	0.05	–3.09	0.00	3.38	0.00	11.16	0.00
R8	1.8	0.10	0.33	–0.94	–3.42	0.07	–5.08	0.02
R9	–0.45	1.82	–0.18	0.00	–5.69	12.42	–3.93	9.26
R10	–0.45	–0.05	–0.18	–0.03	–5.69	–0.16	–3.93	–0.03
R11	–0.45	–0.42	–5.26	10.03	0.31	–0.01	–0.81	–0.02
R12	–0.45	–0.16	0.4	0.03	0.31	–0.20	–0.81	–0.06
R13	1.42	–0.32	–0.49	0.00	–27.56	0.18	–8.9	–0.03
R14	–2.32	–0.26	–4.36	0.03	0.06	0.02	–12.2	0.00
R15	–0.71	1.80	1.51	–0.27	–2.97	4.11	4.15	–4.51
R16	2.09	–1.00	0.82	0.42	10.47	–9.33	0.87	–1.23
R17	–0.28	1.37	1.99	–0.75	–0.89	2.03	6.47	–6.83
R18	0.8	0.29	0.21	1.03	4.31	–3.17	–2.09	1.73
R19	–0.13	1.22	0.66	0.58	–0.17	1.31	0.07	–0.43
RMSE	1.211	0.776	2.420	2.336	9.054	3.798	7.496	2.879
R^2	0.998	0.999	0.991	0.999	0.993	0.999	0.997	0.999

models indicates better performance of the ANN models. In fact, the superiority of the ANN lies in the fact that the models were arrived via splitting the data – despite the few number of experimental runs – which established their credibility. Additionally, as the RSM possess the merit of yielding specific equation capable of predicting and displaying operating parameters influence and their interactions on target response via specific experimental design, the ANN requires neither function nor an experimental design. Nevertheless, both the two approaches predicted well the experimental results in the present study with higher R^2 and low RMSE. Therefore both RSM and ANN model is reliable to interpret EBT adsorption using CO-Al-LDH and B-CoAl-LDH.

3.7. Isotherms analysis of the adsorbent

The phenomena of equilibrium distribution of anionic adsorbate between aqueous phase and the adsorbent surface can be well explained by using models describing the isotherm. Thus, two widely used models namely, Langmuir and Freundlich and models (Eqs. (10) and (11), respectively) were fitted to the equilibrium data to accurately describe the EBT adsorption process.

$$\ln q_e = \ln K_f + \frac{1}{n}\ln C_e \tag{10}$$

$$\frac{C_e}{q_e} = \frac{1}{b}q_m + \frac{C_e}{q_m} \tag{11}$$

Fig. 9 depicts the non-linear plots of isotherm models with experimental values at two studied temperatures and their respective estimated parameters are listed in Table 6. Based on regression coefficient (R^2) values, for two adsorbents, Langmuir isotherm model showed lower values relative to Freundlich model. The higher $R^2 > 0.994$ indicate that the Freundlich isotherm model can adequately describe the EBT adsorption onto CoAl and B-CoAl. Inferably, the EBT adsorption onto CoAl and B-CoAl was explained as a multilayer adsorption in nature. The maximum monolayer adsorption capacity of the CoAl and B-CoAl at 298 K was found to be 323.45 and 609.15 mg/g, respectively. Additionally, Freundlich heterogeneity parameter ($1/n$), decreased with increasing adsorption temperature demonstrating that the EBT adsorption is exothermic in nature and unfavorable at elevated temperatures.

3.8. Regeneration and reusability potentials

The successful industrial application of any adsorbent is mainly evaluated on the basis of its regeneration and reuse performance. The reusability performance of CoAl and B-CoAl was evaluated by conducting series of adsorption–desorption experiments. To achieve that, a basic solution of

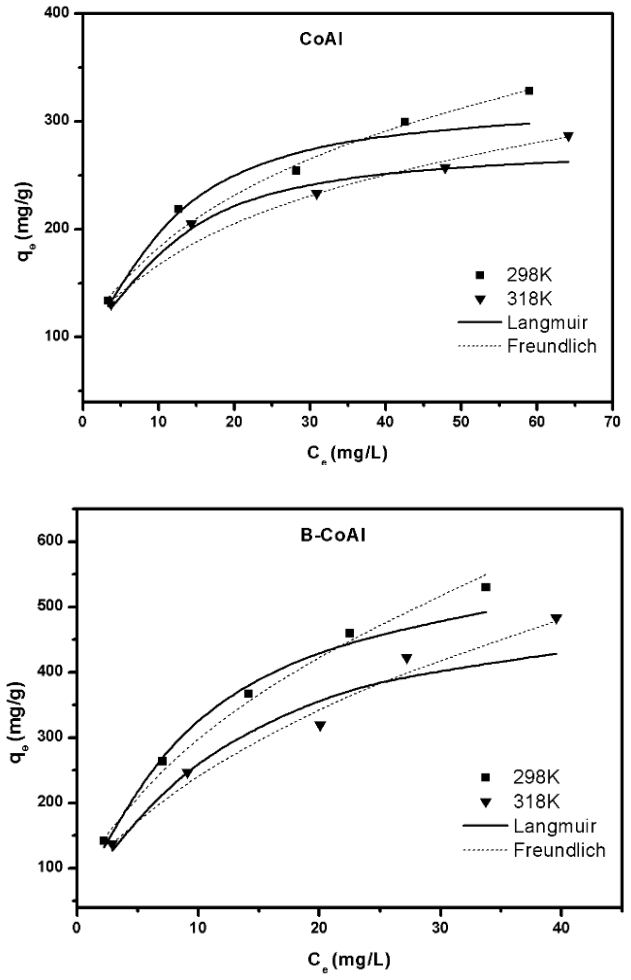

Fig. 9. Langmuir and Freundlich isotherms fittings for CoAl and B-CoAl.

Table 6
Parameters of non-linear Langmuir and Freundlich isotherm models for adsorption of EBT onto B-CoAl-LDH composites

	T (K)	Langmuir			Freundlich		
		q_{max} (mg/g)	K_L	R^2	K_F	1/n	R^2
CoAl	298	323.45	0.20	0.979	94.69	0.30	0.994
	318	280.94	0.22	0.987	94.63	0.26	0.994
B-CoAl	298	609.15	0.12	0.978	98.90	0.48	0.996
	318	526.67	0.11	0.954	82.98	0.47	0.988

0.1 M NaOH was used to desorb EBT dye and effectively regenerate the CoAl and B-CoAl composites. Nearly, 20 mg of each adsorbent was agitated with 200 mL, EBT solution of initial concentration 20 mg/L and pH 2, for about 3 h. The spent adsorbents were regenerated by agitating with 50 mL of basic solution for 2 h. The resulting adsorbent was then thoroughly cleaned times with DI water and allowed to dry at 80°C for 3 h. The adsorbent regenerated was then used for second adsorption test following the procedure mentioned above. The spent adsorbent regeneration–reuse cycle was consecutively repeated three times for the same material. Fig. 10 depicts the percentage removal of EBT after three regeneration–reuse cycles. The results showed that, after three cycles, the removal performance of EBT dyes reduced from 84.23% to 62.66% and 89.93% to 74.55% for CoAl and B-CoAl, respectively. Thus, B-CoAl showed excellent tendency of reuse and can be efficiently and economically employed for eliminating dyes in water and wastewater.

3.9. Comparison with other adsorbents

The performances of the tested B-Co-Al-LDH for EBT sorption was compared with that of other adsorbent materials as obtained from literature under similar experimental conditions (Table 7). As shown in the Table 7, the optimal achieved EBT adsorption capacity for B-Co-Al-LDH of 530 mg/g was relatively higher that the values reported for calcined-AlMg-LDH and calcined-AlCo-LDH [23,25,41–42].

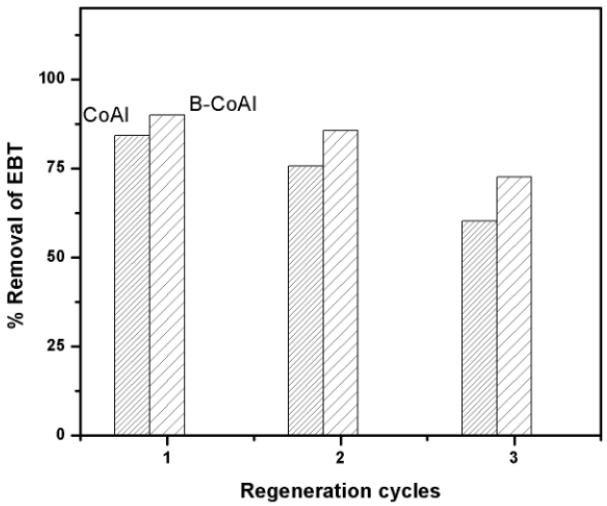

Fig. 10. Three consecutive regeneration and reuse cycle for CoAl and B-CoAl.

Table 7
B-CoAl-LDH adsorption capacity for EBT compared with other adsorbents

Adsorbent	Maximum capacity (mg/g)	References
CuMgAl-LDH	90.5	[[41]]
Magnetite/pectin nanoparticles	72.35	[42]
Date palm ash-MgAl-LDH	425.16	[23]
Graphene	102.04	[40]
Acid-Modified Graphene	70.42	[40]
Calcined NiFe-LDH	132	[25]
Uncalcined-CoAl-LDH	328.8	Present work
Calcined CoAl-LDH	419.25	[25]
Bentonite-CoAl-LDH	530	Present work
MgAl-LDH	540	[25]

Inferably, the synthesized B-CoAl-LDH reported in this study exhibited higher adsorption capacity for EBT. This suggests that this adsorbent has great potentials for effective uptake of anionic dyes from industrial contaminated water. This can be attributed to the improved adsorptive performance observed due to the bentonite hybridization.

4. Conclusion

Bentonite ultrasonicated LDH synthesized using co-precipitation was employed for EBT removal from water. The adsorption process was modeled, evaluated and optimized using RSM under different operational conditions. The predictive performances of the RSM models (removal and adsorption capacity) were compared with that ANN models. RSM and ANN models predictive performances were comparatively, evaluated based on coefficient of determination (R^2) and RMSE. The maximum removal efficiency and adsorption capacities data obtained for the adsorbents well fitted cubic RSM models with insignificant lack of fit (R^2 = 0.991–0.997). The adsorption capacity increased with decrease in pH and increased with initial EBT concentration and tends to decrease with increase in temperature. The maximum achievable EBT adsorption capacity was profoundly raised by a factor of 2.5 and 3.75 to 328.8 and 530 mg/g for an increase in the EBT initial dye concentration from 20 to 100 mg/L, respectively. Both the RSM and ANN models yielded good predictive performances of EBT adsorption by CO-Al-LDH and B-CoAl-LDH with the ANN models (All R^2 = 0.999) exhibiting superior performances. The synthesized B-CoAl-LDH exhibited higher adsorption capacity for EBT compared with other LDH. These results and the excellent regeneration–reuse of the spent adsorbents showed the excellent tendency for their efficient use for eliminating dyes in water and wastewater, economically.

Symbols

A	—	Temperature in °C
ANOVA	—	Analysis of variance
B	—	Initial EBT concentration in mg/L
C	—	Initial pH
EBT	—	Eriochrome Black T
CoAl-LDH	—	Cobolt aluminium doubled layer hydroxide
B-CoAl	—	Bentonite-supported CoAl-LDH
RSM	—	Response surface methodology
FC-CCD	—	Faced centered central composite design
k	—	Number of independent variables
y	—	Model's predicted response
β_0, β_i, β_{ij}, β_{ii}	—	Model's coefficients
x_i, x_j	—	Coded experimental independent variables
C_0	—	Initial concentration of EBT, mg/L
C_f	—	Final concentration of EBT, mg/L
q_e	—	Uptake capacity, mg/g
W	—	Mass of the adsorbent, g
R	—	EBT removal efficiency
V_L	—	Adsorbate solution volume in L
Y_1	—	CoAl EBT removal efficiency, %
Y_2	—	B-CoAl EBT removal efficiency, %
Y_3	—	CoAl EBT adsorption capacity, mg/L
Y_4	—	B-CoAl EBT adsorption capacity, mg/L

Acknowledgments

The King Abdulaziz City for Science and Technology (KACST) funding for Project No. 12-Env2229-46 under NSTIP through at Imam Abdulrahman Bin Faisal University. Also the support provided by the Center of Research Excellences in Nanotechnology King Fahd University of Petroleum & Minerals for synthesis and characterization of the adsorbents is appreciated.

References

[1] Z.P. Xu, J. Zhang, M.O. Adebajo, H. Zhang, C. Zhou, Catalytic applications of layered double hydroxides and derivatives, Appl. Clay Sci., 53 (2011) 139–150.
[2] Y. Kuthati, R.K. Kankala, C.-H. Lee, Layered double hydroxide nanoparticles for biomedical applications: current status and recent prospects, Appl. Clay Sci., 112–113 (2015) 100–116.
[3] M. Daud, M.S. Kamal, F. Shehzad, M.A. Al-Harthi, Graphene/layered double hydroxides nanocomposites: a review of recent progress in synthesis and applications, Carbon, 104 (2016) 241–252.
[4] K.-H. Goh, T.-T. Lim, Z. Dong, Application of layered double hydroxides for removal of oxyanions: a review, Water Res., 42 (2008) 1343–1368.
[5] M. Sajid, C. Basheer, Layered double hydroxides: Emerging sorbent materials for analytical extractions, TRAC-Trend Anal. Chem., 75 (2016) 174–182.
[6] N.N. Das, J. Konar, M.K. Mohanta, S.C. Srivastava, Adsorption of Cr(VI) and Se(IV) from their aqueous solutions onto Zr^{4+}-substituted ZnAl/MgAl-layered double hydroxides: effect of Zr^{4+} substitution in the layer, J. Colloid Interface Sci., 270 (2004) 1–8.
[7] M. Zubair, M. Daud, G. McKay, F. Shehzad, M.A. Al-Harthi, Recent progress in layered double hydroxides (LDH)-containing hybrids as adsorbents for water remediation, Appl. Clay Sci., 143 (2017) 279–292.
[8] W. Peng, H. Li, Y. Liu, S. Song, A review on heavy metal ions adsorption from water by graphene oxide and its composites, J. Mol. Liq., 230 (2017) 496–504.
[9] G. Huang, L. Jiang, D. Wang, J. Chen, Z. Li, S. Ma, Intercalation of thiacalix[4]arene anion via calcined/restored reaction into LDH and efficient heavy metal capture, J. Mol. Liq., 220 (2016) 346–353.
[10] S. Yang, L. Wang, X. Zhang, W. Yang, G. Song, Enhanced adsorption of Congo red dye by functionalized carbon nanotube/mixed metal oxides nanocomposites derived from layered double hydroxide precursor, Chem. Eng. J., 275 (2015) 315–321.
[11] M. Zhang, Q. Yao, C. Lu, Z. Li, W. Wang, Layered double hydroxide–carbon dot composite: high-performance adsorbent for removal of anionic organic dye, ACS Appl. Mater. Interfaces, 6 (2014) 20225–20233.
[12] T.S. Kazeem, M. Zubair, M. Daud, N.D. Mu'azu, M.A. Al-Harthi, Graphene/ternary layered double hydroxide composites: efficient removal of anionic dye from aqueous phase, Korean J. Chem. Eng., 36 (2019) 1057–1068.
[13] N.D. Mu'azu, S.A. Haladu, N. Jarrah, M. Zubair, M.H. Essa, S.A. Ali, Polyaspartate extraction of cadmium ions from contaminated soil: Evaluation and optimization using central composite design, J. Hazard. Mater., 342 (2018) 58–68.
[14] R.H. Myers, D.C. Montgomery, C.M. Anderson-Cook, Response Surface Methodology: Process and Product Optimization Using Designed Experiments, John Wiley & Sons, Productivity Press, New York, 2016.
[15] G. Astray, B. Gullón, J. Labidi, P. Gullón, Comparison between developed models using response surface methodology (RSM) and artificial neural networks (ANNs) with the purpose to optimize oligosaccharide mixtures production from sugar beet pulp, Ind. Crops Prod., 92 (2016) 290–299.
[16] J.L. Pilkington, C. Preston, R.L. Gomes, Comparison of response surface methodology (RSM) and artificial neural

networks (ANN) towards efficient extraction of artemisinin from *Artemisia annua*, Ind. Crops Prod., 58 (2014) 15–24.
[17] G. Sodeifian, S.A. Sajadian, N. Saadati Ardestani, Evaluation of the response surface and hybrid artificial neural network-genetic algorithm methodologies to determine extraction yield of *Ferulago angulata* through supercritical fluid, J. Taiwan Inst. Chem. Eng., 60 (2016) 165–173.
[18] Z. Kim, Y. Shin, J. Yu, G. Kim, S. Hwang, Development of NOx removal process for LNG evaporation system: comparative assessment between response surface methodology (RSM) and artificial neural network (ANN), J. Ind. Eng. Chem., 74 (2019) 136–147.
[19] S. Muthusamy, L.P. Manickam, V. Murugesan, C. Muthukumaran, A. Pugazhendhi, Pectin extraction from *Helianthus annuus* (sunflower) heads using RSM and ANN modelling by a genetic algorithm approach, Int. J. Biol. Macromol., 124 (2019) 750–758.
[20] K. Ameer, B.-S. Chun, J.-H. Kwon, Optimization of supercritical fluid extraction of steviol glycosides and total phenolic content from *Stevia rebaudiana* (Bertoni) leaves using response surface methodology and artificial neural network modeling, Ind. Crop Prod., 109 (2017) 672–685.
[21] M.R. Gadekar, M.M. Ahammed, Modelling dye removal by adsorption onto water treatment residuals using combined response surface methodology-artificial neural network approach, J. Environ. Manage., 231 (2019) 241–248.
[22] N. Jarrah, N.D. Mu'azu, M. Zubair, M. Al-Harthi, Enhanced adsorptive performance of Cr(VI) onto layered double hydroxide-bentonite composite: isotherm, kinetic and thermodynamic studies, Sep. Sci. Technol., (2019) 1–13.
[23] N.I. Blaisi, M. Zubair, Date palm ash-MgAl-layered double hydroxide composite: sustainable adsorbent for effective removal of methyl orange and eriochrome black-T from aqueous phase, Environ. Sci. Pollut. Res., 25 (2018) 34319–34331.
[24] X. Wu, B. Li, X. Wen, Synthesis and adsorption properties of hierarchical Fe_3O_4@MgAl-LDH magnetic microspheres, J. Nanopart. Res., 19 (2017) 131.
[25] M. Zubair, N. Jarrah, M.S. Manzar, M. Al-Harthi, M. Daud, N.D. Mu'azu, S.A. Haladu, Adsorption of eriochrome black T from aqueous phase on MgAl-, CoAl- and NiFe- calcined layered double hydroxides: kinetic, equilibrium and thermodynamic studies, J. Mol. Liq., 230 (2017) 344–352.
[26] M.H. Essa, N.D. Mu'azu, S. Lukman, A. Bukhari, Application of Box-Behnken Design to hybrid electrokinetic-adsorption removal of mercury from contaminated saline-sodic clay soil, Soil Sedim. Contam., 24 (2015) 30–48.
[27] N.D. Mu'azu, M.H. Al-Malack, N. Jarrah, Electrochemical oxidation of low phenol concentration on boron doped diamond anodes: optimization via response surface methodology, Desal. Wat. Treat., 52 (2014) 7293–7305.
[28] R.H. Myers, D.C. Montgomery, Response Surface Methodology: Process and Product Optimization Using Designed Experiments, 1st ed., John Wiley & Sons Inc, New York, 1995.
[29] Y. Vlamidis, E. Scavetta, M. Giorgetti, N. Sangiorgi, D. Tonelli, Electrochemically synthesized cobalt redox active layered double hydroxides for supercapacitors development, Appl. Clay Sci., 143 (2017) 151–158.
[30] M. Hussein, A. Jaafar, A. Yahaya, M. Masarudin, Z. Zainal, Formation and Yield of Multi-Walled Carbon Nanotubes Synthesized via Chemical Vapour Deposition Routes Using Different Metal-Based Catalysts of FeCoNiAl, CoNiAl and FeNiAl-LDH, Int. J. Mol. Sci., 15 (2014) 20254.
[31] N.D. Mu'azu, A. Usman, N. Jarrah, O. Alagha, Pulsed Electrokinetic Removal of chromium, mercury and cadmium from contaminated mixed clay soils, Soil Sedim. Contam., 25 (2016) 757–775.
[32] G. Wang, S. Zhang, T. Li, X. Xu, Q. Zhong, Y. Chen, O. Deng, Y. Li, Application of response surface methodology for the optimization of lead removal from contaminated soil using chelants, RSC Adv., 5 (2015) 58010–58018.
[33] G. Wang, S. Zhang, X. Xu, Q. Zhong, C. Zhang, Y. Jia, T. Li, O. Deng, Y. Li, Heavy metal removal by GLDA washing: optimization, redistribution, recycling, and changes in soil fertility, Sci. Total Environ., 569–570 (2016) 557–568.
[34] A.A. Oladipo, M. Gazi, Enhanced removal of crystal violet by low cost alginate/acid activated bentonite composite beads: optimization and modelling using non-linear regression technique, J. Water Process Eng., 2 (2014) 43–52.
[35] Y. Lu, B. Jiang, L. Fang, F. Ling, J. Gao, F. Wu, X. Zhang, High performance NiFe layered double hydroxide for methyl orange dye and Cr (VI) adsorption, Chemosphere, 152 (2016) 415–422.
[36] F.B.D. Saiah, B.-L. Su, N. Bettahar, Nickel–iron layered double hydroxide (LDH): textural properties upon hydrothermal treatments and application on dye sorption, J. Hazard. Mater., 165 (2009) 206–217.
[37] L. Lu, J. Li, D.H. Ng, P. Yang, P. Song, M. Zuo, Synthesis of novel hierarchically porous Fe_3O_4@ MgAl–LDH magnetic microspheres and its superb adsorption properties of dye from water, J. Ind. Eng. Chem., 46 (2017) 315–323.
[38] N. Belhouchat, H. Zaghouane-Boudiaf, C. Viseras, Removal of anionic and cationic dyes from aqueous solution with activated organo-bentonite/sodium alginate encapsulated beads, Appl. Clay Sci., 135 (2017) 9–15.
[39] L. Lu, J. Li, D.H.L. Ng, P. Yang, P. Song, M. Zuo, Synthesis of novel hierarchically porous Fe_3O_4@MgAl–LDH magnetic microspheres and its superb adsorption properties of dye from water, J. Ind. Eng. Chem., 46 (2017) 315–323.
[40] A. Khalid, M. Zubair, A comparative study on the adsorption of Eriochrome Black T dye from aqueous solution on graphene and acid-modified graphene, Arab. J. Sci. Eng., 43 (2017) 2167–2179.
[41] D. Bharali, R.C. Deka, Preferential adsorption of various anionic and cationic dyes from aqueous solution over ternary CuMgAl layered double hydroxide, Colloids Surf., A, 525 (2017) 64–76.
[42] O.A. Attallah, M.A. Al-Ghobashy, M. Nebsen, M.Y. Salem, Removal of cationic and anionic dyes from aqueous solution with magnetite/pectin and magnetite/silica/pectin hybrid nanocomposites: kinetic, isotherm and mechanism analysis, RSC Adv., 6 (2016) 11461–11480.

Supplementary information

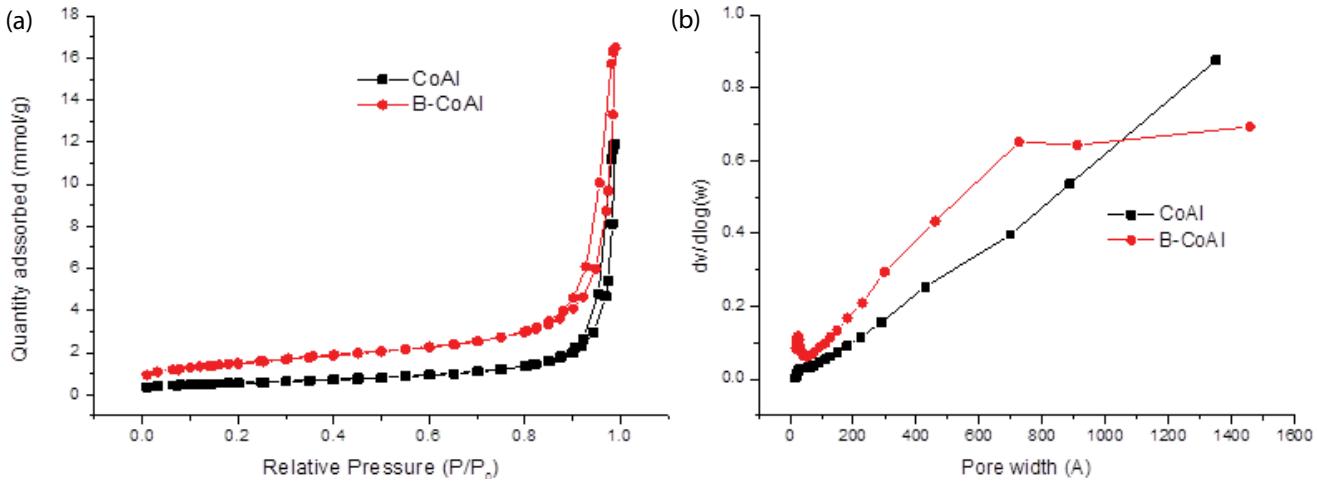

Fig. S1. Mesoporous CoAl and bentonite-CoAl (a) distribution of pore size and (b) N_2 isotherm for adsorption–desorption.

Table S1
CoAl and bentonite-CoAl mesoporous characteristics

LDH	BET surface area (m^2/g)	Pore volume (cm^3/g)	Pore size (A)
CoAl	44.2	0.02	34.6
B-CoAl	119.1	0.06	19.5

Table S2
Composition of Co-Al and bentonite-CoAl and bentonite

Materials	Elemental weight (%)											
	C	O	Na	Mg	Al	Si	Cl	Ca	Fe	Co	Cu	Total
Bentonite	13.87	51.83	1.16	1.33	7.47	18.22	1.06	0.56	2.66	–	1.85	100
	20.83	58.42	0.91	0.99	4.99	11.7	0.54	0.25	0.86	–	0.52	100
Co-Al	–	24.69	–	–	5.72	–	–	–	–	69.59	–	100
	–	52.56	–	–	7.22	–	–	–	–	40.22	–	100
B-CoAl	8.68	39.12	–	–	6.54	2.64	–	–	–	40.36	2.66	100
	17.08	57.79	–	–	5.73	2.23	–	–	–	16.19	0.99	100